Optimal design of one-dimensional photonic crystal back reflectors for thin-film silicon solar cells

Peizhuan Chen, Guofu Hou,[a] Jianjun Zhang,[b] Xiaodan Zhang, and Ying Zhao
Institute of Photoelectronics and Tianjin Key Laboratory of Photoelectronic Thin-film Devices and Technique, Nankai University, Tianjin 300071, People's Republic of China

(Received 10 April 2014; accepted 4 August 2014; published online 14 August 2014)

For thin-film silicon solar cells (TFSC), a one-dimensional photonic crystal (1D PC) is a good back reflector (BR) because it increases the total internal reflection at the back surface. We used the plane-wave expansion method and the finite difference time domain (FDTD) algorithm to simulate and analyze the photonic bandgap (PBG), the reflection and the absorption properties of a 1D PC and to further explore the optimal 1D PC design for use in hydrogenated amorphous silicon (a-Si:H) solar cells. With identified refractive index contrast and period thickness, we found that the PBG and the reflection of a 1D PC are strongly influenced by the contrast in bilayer thickness. Additionally, light coupled to the top three periods of the 1D PC and was absorbed if one of the bilayers was absorptive. By decreasing the thickness contrast of the absorptive layer relative to the non-absorptive layer, an average reflectivity of 96.7% was achieved for a 1D PC alternatively stacked with a-Si:H and SiO_2 in five periods. This reflectivity was superior to a distributed Bragg reflector (DBR) structure with 93.5% and an Ag film with 93.4%. *n-i-p* a-Si:H solar cells with an optimal 1D PC-based BR offer a higher short-circuit current density than those with a DBR-based BR or an AZO/Ag-based BR. These results provide new design rules for photonic structures in TFSC. © *2014 AIP Publishing LLC*. [http://dx.doi.org/10.1063/1.4893180]

I. INTRODUCTION

Thin-film silicon solar cells (TFSC) are promising candidates for the global terawatt-scale deployment of photovoltaics because of the abundance and non-toxicity of raw materials, and mature fabrication processes.[1,2] One of the foremost challenges in designing TFSC is to devise an efficient light trapping system because of the short optical path length imposed by the inherent thin absorption layers.[3,4] For the *n-i-p* configuration, the strategy relies on the deposition of a thin ITO front contact, which acts as an antireflection layer,[5] and a randomly textured[6] or an in-plane structure photonic crystal (PC) based metallic back reflector (BR),[7,8] which is commonly used to reflect and scatter light within the absorber. Conventional BRs of silver (Ag) coated with ZnO suffer from intrinsic losses of surface plasmon modes that are generated at the granular metal-dielectric interface.[9] These losses accumulate for every reflection within the active layer and become severe at a higher photon wavelength as multiple optical passes are required.[10]

An alternative, highly promising approach is to use a dielectric one-dimensional (1D) PC, which is a multilayer structure in which two layers (bilayers) with a high refractive index contrast are periodically stacked.[11,12] The periodic refractive index causes the electromagnetic waves within the PC to diffract and form interference patterns, giving rise to many interesting optical phenomena such as the superprism effect, slow photons and a photonic bandgap (PBG).[13] The PBG is a frequency range wherein the interference pattern of the electromagnetic waves is destructive along all directions and light within it is thus prevented from propagating.[14] The combination of a transparent conductive oxide (TCO) layer and a 1D PC can simultaneously serve as the back electrical contact and the BR in a TFSC. Unwanted intrinsic losses are thus avoided because of surface plasmon modes. In previous work, a 1D PC BR was used as a distributed Bragg reflector (DBR), in which the thickness of the individual layers were calculated on a quarter-wavelength basis for the Bragg wavelength λ_0.[12,15,16] Additionally, light propagation within the bulk of the PC was assumed to be forbidden, which led to the assumption that 100% frequency reflection occurred within the PBG because the light impinging onto the PC surface must be reflected.[13,17] Both these ideas prevented the determination of an optimized PC configuration, especially if at least one of the bilayers is absorptive within the PBG, thus limiting the application of 1D PC in TFSC.

Here, we discuss a different approach for the determination of an optimized 1D PC design and parameters for an a-Si:H TFSC using commercial finite difference time domain (FDTD) software. We focused on flat *n-i-p* structures as a convenient prototype but all the modeling could apply to *p-i-n* devices and tandem TFSC in the same manner. To enable the PBG to cover the light trapping range required for an a-Si:H TFSC, the influence of bilayer thickness contrast and the corresponding period on the PBG were investigated using the plane-wave expansion method (PWEM). A general roadmap for the use of 1D PC and TCO to achieve the highest absorption in the active layer and the highest short-circuit current density (J_{sc}) from an optical point of view is outlined based on the FDTD algorithm.

[a]Author to whom correspondence should be addressed. Electronic mail: gfhou@nankai.edu.cn
[b]E-mail: jjzhang@nankai.edu.cn

II. MODELING AND ANALYSIS

PWEM is a popular technique for the calculation of the band structure of periodic devices in which the structures extend periodically in all dimensions.[18] Figure 1 shows a schematic diagram of a 1D PC with a lower refractive index layer on top and a higher refractive index layer at the bottom. The band solution for such a 1D PC assumes periodicity in the z-direction and the boundary conditions of the x- and y-directions are set with perfectly matched layers (PML). To perform band calculations, a defined K-vector path is specified in terms of reciprocal lattice vectors. The first vector has a number of divisions that are automatically set to 1 as there is no vector in the k-path preceding it. Figure 2 shows the band diagram populated with a set of eigenfrequencies of individual k-vectors. The calculated eigenfrequencies are plotted in a normalized fashion as $f = \omega/2\pi c$ in units of $1/\mu$m, where ω is the frequency, c is the speed of light in free space; this is not the same as that reported for a non-dimensional form ($\omega a/2\pi c$) because the lattice constant a is set to 1 μm. The normalized frequency can be readily transformed into wavelength in microns using $\lambda = 1/f$. Therefore, the first PBG in Fig. 2 lies in a wavelength range between 497 nm and 909 nm. If we refer to these two wavelengths as Band0 and Band1, respectively, then the first PBG described by the wavelength range is given by Band1 minus Band0, which is about 412 nm. Because it is the widest band and can be translated to the solar spectrum region where it is most beneficial for TFSC (300–1100 nm), only the first PBG will be studied (including its boundary, band0 and band1) using the following PWEM calculation.

The FDTD has become a state-of-the-art method to solve Maxwell's equations for complex geometries.[19] In this letter, the FDTD algorithm was used to calculate the reflection, the electric field intensity $|E|^2$ distribution, the absorption of individual layers in the 1D PC and the quantum efficiency of the solar cell, QE (λ). By assuming that all electron-hole pairs contribute to the photocurrent, the short

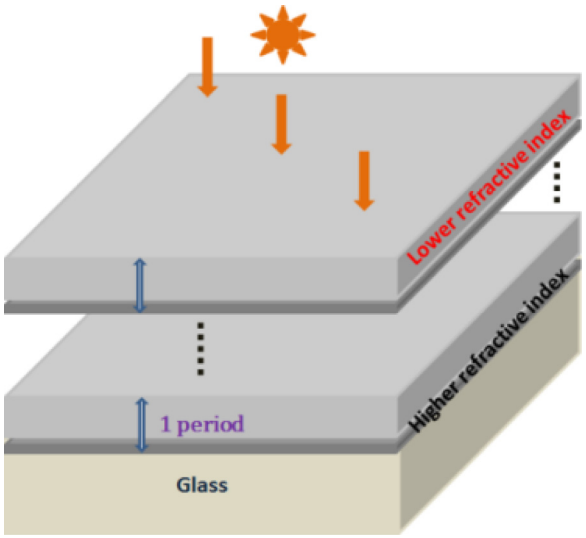

FIG. 1. Schematic of a 1D PC structure with bilayers of a lower refractive index layer on top and a higher refractive index layer at the bottom.

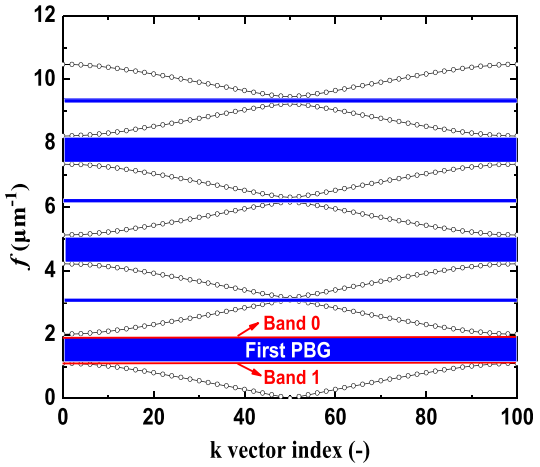

FIG. 2. Band diagram of a 1D PC where the blue region represents the PBG.

circuit current density J_{sc} of the solar cell can be determined by:

$$J_{SC} = e\int \frac{\lambda}{hc} QE(\lambda) I_{AM1.5}(\lambda) d\lambda, \tag{1}$$

where e is the charge on an electron, h is Plank's constant, c is the speed of light in free space and $I_{\mathrm{AM1.5}}$ is the AM1.5 solar spectrum. The $I_{\mathrm{AM1.5}}$ data are taken from the reference ASTM G173-03 spectrum, as published by the National Renewable Energy Laboratory (NREL).[20] We assume that one photon generates one electron-hole pair and that all the electrons and holes are fully collected by the electrode. Therefore, the $QE(\lambda)$ is defined as:

$$QE(\lambda) = \frac{\frac{P_{abs}(\lambda)\lambda}{hc} \times 1 \times 1}{\frac{P_{in}(\lambda)\lambda}{hc}} = \frac{P_{abs}(\lambda)}{P_{in}(\lambda)}, \tag{2}$$

where $P_{in}(\lambda)$ and $P_{abs}(\lambda)$ are the power of the incident light and the absorbed light within the intrinsic layer of the a-Si:H TFSC, respectively, at a wavelength λ. To calculate the P_{abs} as a function of space and frequency, ω, we only need to know the electric field intensity $|E|^2$ and the imaginary part of the permittivity $imag(\varepsilon)$ according to Eq. (3).[21] Both quantities are easily measured for the FDTD simulation

$$P_{abs} = -0.5\omega |E|^2 imag(\varepsilon). \tag{3}$$

The optical constants as a function of wavelength for each of the materials used in the simulation were measured in our laboratory by ellipsometry, WVASE32 and then fit to the FDTD data by a multi-coefficient model, which accurately accounts for broadband linear material dispersion.

III. RESULTS AND DISCUSSION

A. Influence of bilayer thickness contrast on the PBG

In the following simulation, one of the dielectric layers used was SiO_2 because of its transparency, non-dispersion, lower refractive index of 1.5 and its deposition process

compatibility with TFSC. From the PWEM calculation, we found that the incident medium and the stacking order of the two dielectric layers has nearly no influence on the PBG. Therefore, in the following discussion the incident medium was set to air and the stacking order was a lower refractive index layer on top and a higher refractive index layer at the bottom, as shown in Fig. 1.

It is difficult to get a PBG to cover the whole absorption wavelength range from 300 to 800 nm for an a-Si:H TFSC because of the limited index contrast of the bilayers. Therefore, tailoring a suitable light trapping range for TFSC and the corresponding PBG for a 1D PC is important. Figure 3 shows a cross-section image of the $|E|^2$ distribution at incident wavelengths of 510 nm, 520 nm, 530 nm, and 540 nm for an a-Si:H TFSC with a n-μc-SiOx (15 nm)/i-a-Si (400 nm)/p-μc-SiC (15 nm)/ITO (80 nm) structure. Light is incident from the ITO/air interface. From these images, it is clear that the electric field intensity gradually decreases with an increase in depth from the p-layer to the n-layer because of absorption by the intrinsic layer. Only light of higher than 520 nm will arrive at the bottom of the cell (n-layer) where the back reflection starts to work. It is well known that the upper absorption wavelength limit for a-Si:H is located in the wavelength range of 750–800 nm because of its wide bandgap of over 1.6 eV[3]. Therefore, reflected light from the BR outside the wavelength range of 520–800 nm has little effect on TFSC performance. To conclude, the PBG should at least cover the light trapping range of 520–800 nm to enhance absorption in the cell.

As a DBR structure, the average reflectivity in the light trapping range is closely related to the Bragg wavelength λ_0. The period thickness and the corresponding thickness of the higher and the lower refractive index layer can be calculated using the typical Bragg equation. To determine the optimized DBR structure, Fig. 4 shows the average reflectivity in the wavelength range of 520–800 nm and the period thickness as a function of λ_0 for the DBR structure that consists of five periods of an a-Si:H (higher refractive index) layer and a SiO_2 (lower refractive index) layer. We found that the maximum average reflectivity is in the Bragg wavelength range of 600–650 nm, with a corresponding period thickness range of 139–152 nm. For comparison, a period thickness of 150 nm (Bragg wavelength of 640 nm) was employed for a PBG simulation. The thicknesses of the a-Si:H (refractive index of 4 at $\lambda = 640$ nm) and the SiO_2 layers for this optimal DBR structure were 40 nm and 110 nm, respectively.

Because most high refractive index materials are dispersive, the PBG as a function of thickness contrast for three

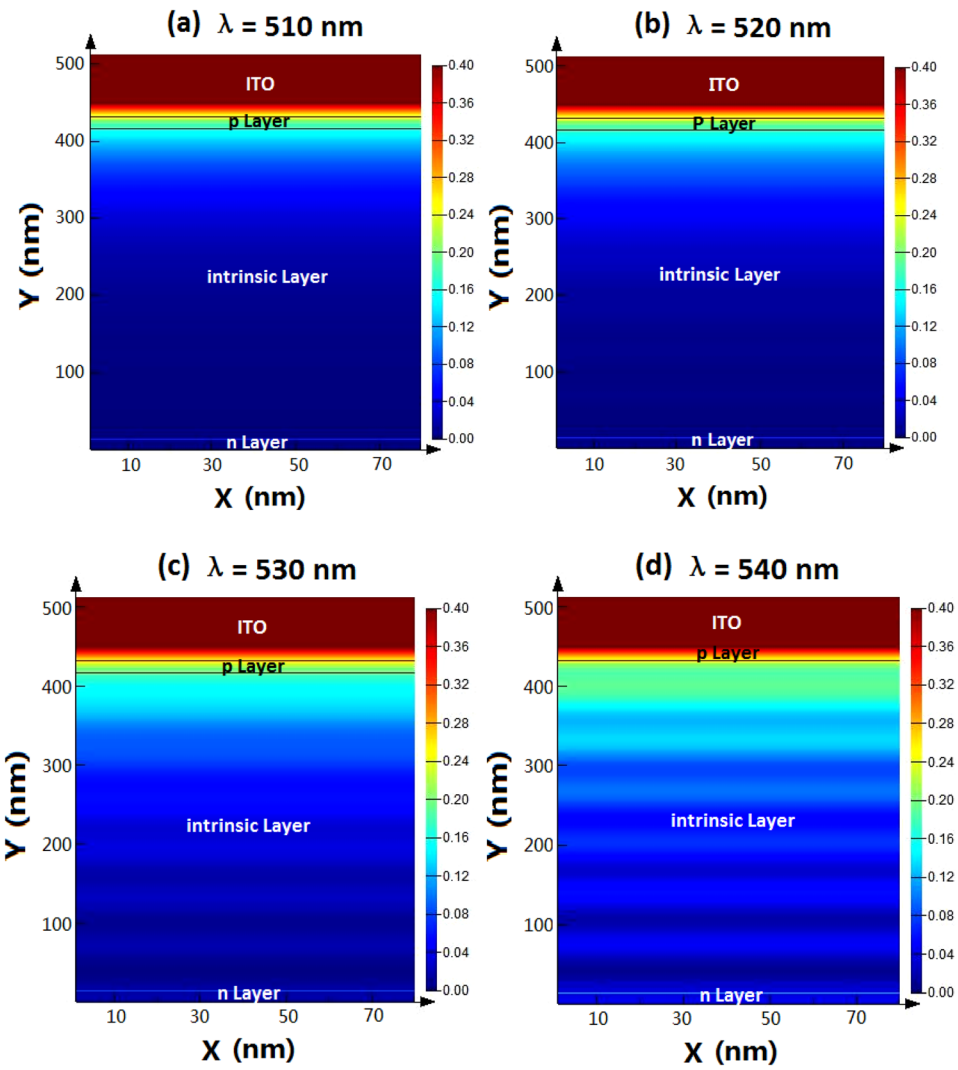

FIG. 3. Cross-section images of the $|E|^2$ distribution for an a-Si:H TFSC with a n-μc-SiOx (15 nm)/i-a-Si (400 nm)/p-μc-SiC (15 nm)/ITO (80 nm) structure at incident wavelengths of (a) 510 nm, (b) 520 nm, (c) 530 nm, and (d) 540 nm.

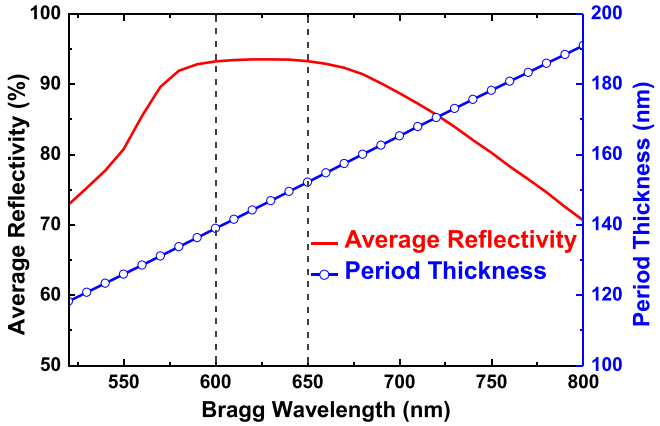

FIG. 4. Average reflectivity in the wavelength range of 520–800 nm and the period thickness as a function of the Bragg wavelength. The DBR structure consists of five periods of an a-Si:H (higher refractive index) layer and a SiO_2 (lower refractive index) layer.

different refractive index contrasts (3/1.5, 4/1.5 and 5/1.5) are given in Fig. 5. The proportions 10/140, 20/130,…, in the x axis indicate that the thickness of the higher and lower refractive index layers are 10 nm and 140 nm, respectively, and then 20 nm and 130 nm, respectively, and so on, while the period thickness of 150 nm is constant. Compared with the lower refractive index contrast, we found that the higher refractive index contrast would result in a wider PBG if the other parameters remain unchanged, which suggests that the higher refractive index contrast of the 1D PCs is most beneficial for TFSC because of the broader PBGs. All three PBG curves exhibited similar tendencies of an initial increase and then a slight decrease with an increase in thickness contrast. If the peaks are connected to obtain the 95% peak value for each refractive index contrast, it is interesting that the peak region of the PBGs shifts parallel to the small thickness contrast values when increasing the refractive index contrast from 3/1.5 to 5/1.5. The widest PBG (95%–100% of the peak value) was obtained at a thickness contrast of 1/2 to 2/3

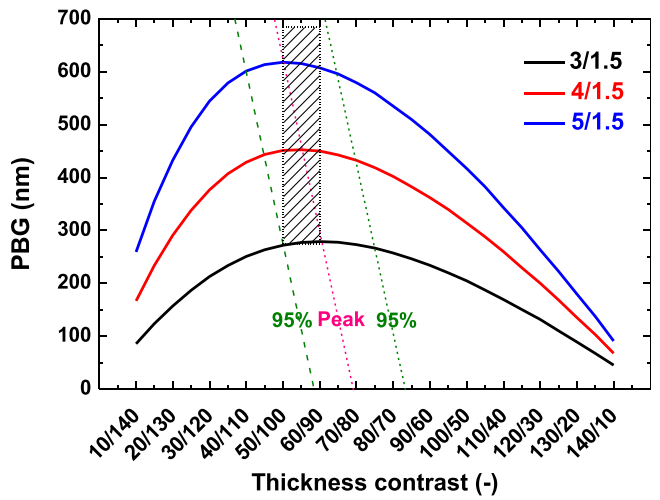

FIG. 5. PBG vs thickness contrast (period thickness 150 nm) for different index contrasts. The proportions 10/140, 20/130,…, in the x axis indicate that the thickness of the higher and lower refractive index layers are 10 nm and 140 nm, respectively, changing to 20 nm and 130 nm and so on while keeping the period thickness constant at 150 nm.

for the refractive index contrast located between 3/1.5 and 5/1.5, as shown in the shaded area of Fig. 5. The same conclusion can be made for a wide range of periods but these are not shown here. Noticeably, the contrast value of 40/110 for the DBR configuration is outside the above-mentioned range, which means that DBR is not necessarily the best manner in which to achieve the broadest PBG for a certain period thickness.

To demonstrate the PBG variation more clearly, Fig. 6 shows a diagram of Band0 and Band1 as a function of the thickness contrast (refractive index contrast of 4/1.5, period thickness of 150 nm). Figure 6 shows that the morphology of PBG opens in an "eye" form with an increase in the thickness contrast value. To cover the light trapping range of 520–800 nm for an a-Si:H TFSC, several thickness contrast values with a range from 30/120 to 50/100 including the DBR structure can be used (see the shaded area in Fig. 6). As expected, many groups of layer thickness contrasts, with a corresponding period thickness around 150 nm, can yield a PBG over a light trapping range of 520–800 nm. In the 1D PC, the PBG center frequency ω_0 can be expressed by the following equation:[22]

$$\omega_0 = c\pi/(n_a a + n_b b), \tag{4}$$

where n_a and n_b are the refractive index of the two dielectric layers, respectively, a and b are their corresponding thicknesses, and c is the speed of light in free space. If n_a and n_b are identified, several groups of a and b satisfy the above-mentioned equation for a certain ω_0 (reciprocal relationship with the center wavelength λ_0). However, as for the DBR structure, only one group of a and b values are obtained for the identified λ_0 according to the Bragg equation. By comparison with DBR, the 1D PC has a higher reflectivity within the PBG because of its flexible layer thickness selection, especially when at least one of the layers is absorptive, as will be discussed later.

When fixing the thickness and refractive index contrast for 1/2 and 4/1.5, respectively, we found that the PBG, Band0 and Band1 linearly increase with an increase in the period thickness, as shown in Fig. 7. Therefore, another good

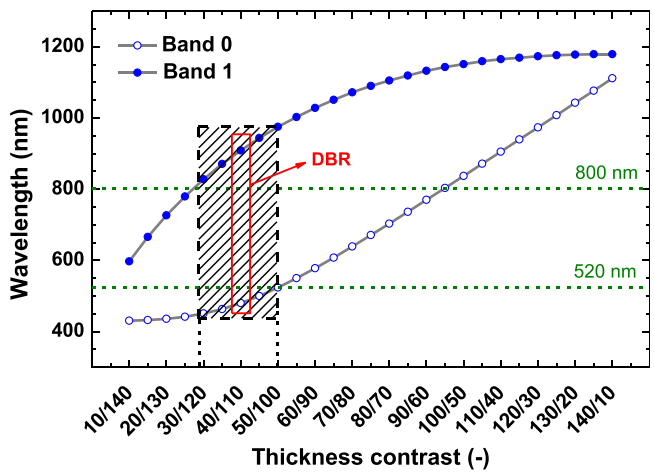

FIG. 6. Morphology of the PBG as a function of thickness contrast (refractive index contrast: 4/1.5, period thickness: 150 nm).

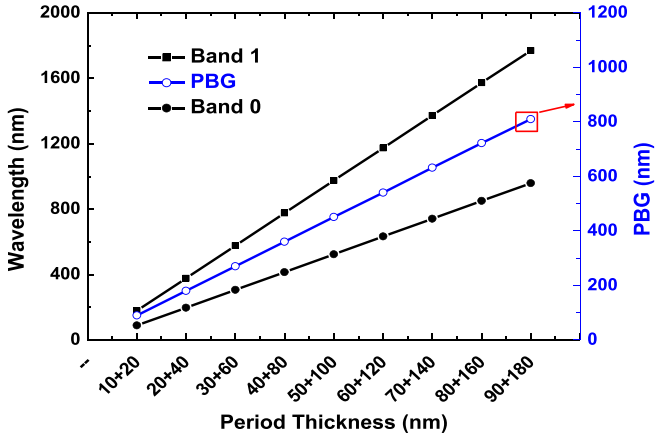

FIG. 7. Variation of PBG, Band0, and Band1 with period thickness (refractive index contrast: 4/1.5, thickness contrast: 1/2). The expressions 10 + 20, 20 + 40,…, in the *x* axis indicate that the thicknesses of the higher and lower refractive index layers are 10 nm and 20 nm (period thickness of 30 nm), respectively, and they shift by 20 nm and 40 nm (period thickness 60 nm) and so on with a period thickness step of 30 nm.

method to increase the PBG is to adopt a larger period thickness. However, care should be taken as the PBG center ([Band1 + Band0]/2) will shift to a longer wavelength.

B. Reflection comparison between the DBR and the optimal 1D PC

To further investigate the difference between DBR and the other 1D PCs, Fig. 8 shows simulated reflection spectra for thickness contrasts of 30 nm/120 nm (higher/lower refractive index layer) and 40 nm/110 nm (one of the optimal DBR structures as shown in Fig. 4) with the same period thickness of 150 nm and the result of 30 nm/140 nm with a period thickness of 170 nm. Reference data for the Ag film and the transmission curve for 30 nm/140 nm(T_30 nm/140 nm) are also listed here. Table I summarizes the corresponding average reflectivity in wavelength ranges of 520–800 nm and 520–620 nm. When applying the 1D PC to an a-Si:H TFSC, it is not easy to obtain two visible light non-absorptive materials with a high refractive index contrast. Here, we used

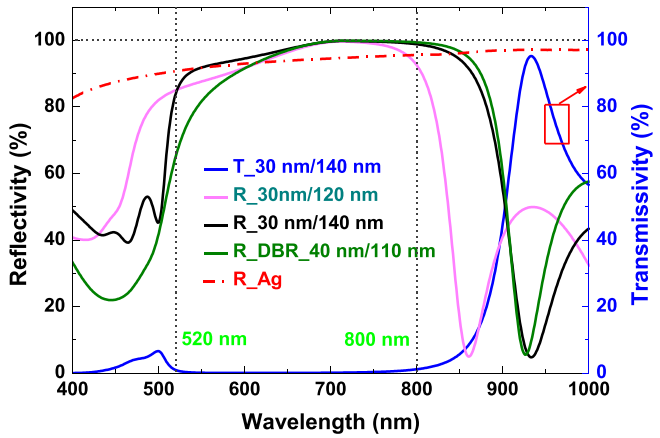

FIG. 8. Simulated reflection curves for thickness contrasts of 30 nm/120 nm (higher/lower refractive index layers), 40 nm/110 nm (DBR structure), 30 nm/140 nm and the Ag film. T_30 nm/140 nm is the transmission curve for 30 nm/140 nm.

TABLE I. Average reflectivities in wavelength ranges of 520–800 nm and 520–620 nm for thickness contrasts of 30 nm/120 nm, 40 nm/110 nm, 30 nm/140 nm and the Ag film.

Wavelength range	30 nm/120 nm	40 nm/110 nm	30 nm/140 nm	Ag
520–800 nm	94.7%	93.5%	96.7%	93.4%
520–620 nm	89.3%	84.7%	92.5%	92.2%

a-Si:H ($n \cong 4$ at a wavelength of 640 nm) and SiO_2 ($n \cong 1.5$) as the higher and lower refractive index materials, respectively, because they are not only compatible with the TFSC deposition process but also provide a sufficient higher index contrast. To make the simulation more realistic, only five periods were used to shorten the fabrication time. Little change was observed for the reflection in the PBG area if the periods were higher than 5 (will be discussed later).

As shown in Fig. 8, the PBG appeared in the wavelength range of 520–800 nm because no transmission was observed from the 1D PC (see the transmission curve of T_30 nm/140 nm). A gradual increase in the PBG was evident for all three thickness contrast reflection curves and nearly 100% reflectivity was achieved around 800 nm. The major difference among these is found in the short wavelength range of 520–620 nm. At the same period thickness of 150 nm, the average reflectivity in the above-mentioned wavelength range decreased with an increase in the thickness contrast, from 89.3% for 30 nm/120 nm to 84.7% for the DBR structure(40 nm/110 nm), which is lower than that of the Ag film of 92.2% (see Table I). However, this reduction can be strongly suppressed by increasing the thickness of the non-absorptive SiO_2 layer while retaining the thickness of the absorptive a-Si:H layer at a constant 30 nm. In other words, the thickness contrast can be decreased further by increasing the period thickness. With a contrast value of 30 nm/140 nm, the 1D PC yielded an average reflectivity of 96.7% over the whole light trapping range, and it thus outperformed the 30 nm/120 nm structure with 94.7%, the Ag film with 93.4%, and the DBR structure with 93.5%.

Nevertheless, in the wavelength range of 520–620 nm an average reflectivity of 100% was not obtained after optimization (92.5%). It seems that the light could transmit into the 1D PC and was absorbed because the transmittance was zero. To verify this, a cross-section image of the $|E|^2$ distribution for the optimized 1D PC at a wavelength of 550 nm (peak absorption wavelength for the a-Si:H) and at 750 nm(band edge for the a-Si:H) are shown in Fig. 9. Power absorption is proportional to electric field intensity according to Eq. (3). Here, light is normally incident from air. Similar images were obtained for the inverse structure with a-Si:H on top and SiO_2 at the bottom. From these images, the following conclusions can be drawn. First, light will definitely couple with the 1D PC irrespective of the material being absorptive or not and most of the light is concentrated in the lower refractive index layers. This suggests that it is essential to select a non-absorptive material in the PBG area for the low-index layer to obtain higher reflectivity. Second, $|E|^2$ decreases significantly from period one to period three and the value is close to zero from the fourth period. The above-mentioned

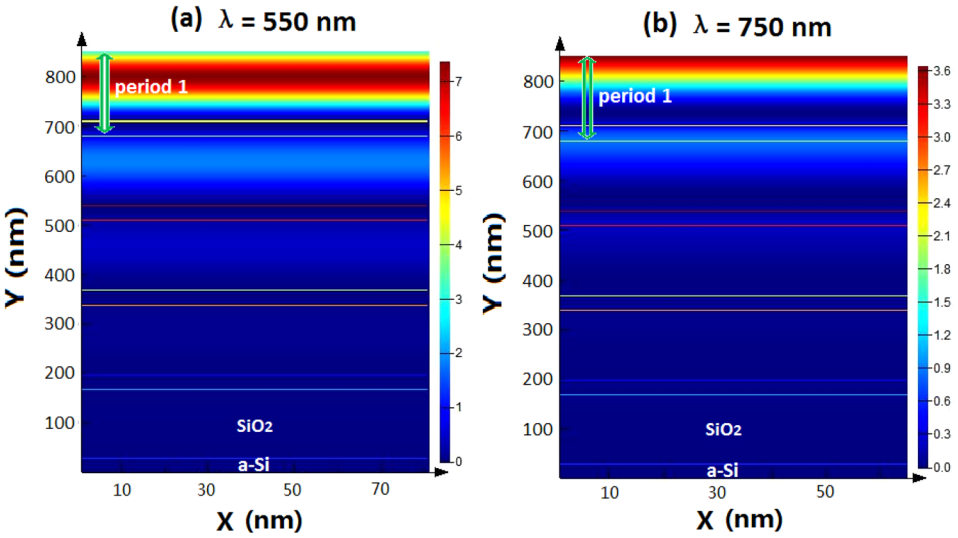

FIG. 9. Cross-section images of the $|E|^2$ distribution for the optimized 1D PC at an incident wavelength of (a) 550 nm and (b) 750 nm.

phenomenon also appears when light is incident from the background refractive index of 2, and 3, etc. (not illustrated here). This indicates that increasing periods beyond four or five will not further enhance the reflectivity. In other words, four or five periods are sufficient to achieve the highest reflection for identical parameters.

To better understand bulk absorption by the 1D PC, Fig. 10 shows absorption spectra for the individual periods from periods 1 to 5. Similarly, absorption within the PBG was only observed for the top three periods and mainly occurs in the first period. It should be noted that this absorption is fully generated in the a-Si:H layer for each of the bilayers as the SiO_2 layer is non-absorptive. The DBR structure has a lower reflectivity over the short wavelength range of 520–620 nm because of its thicker a-Si:H layer (40 nm) compared with the optimized 1D PC (30 nm). Therefore, reducing the thickness of the absorptive layer and increasing the thickness of the non-absorptive layer is an effective way to enhance reflections in the PBG. A further improvement in reflection can be expected by reducing the material's absorption coefficient in the first period. However, if both materials are non-absorptive, a thickness contrast value of 1/2–2/3 is strongly recommended to achieve the widest high reflection region.

For the solar cell application, it is useful to compare the average reflectivity (520–800 nm) of the DBR and the optimized 1D PC as a function of the incident angle of solar radiation, as shown in Fig. 11. In the wavelength range of 520–800 nm, no obvious decrease was observed in the average reflectivity for both structures when the incident angles were smaller than 40°. The average reflectivity decreased quickly as the incident angle increased from 40° to 75°. Finally, a sharp increase is apparent upon a further increase in the angle. The average reflectivity difference between the 1D PC and the DBR decreased for incident angles higher than 40°. Our previous results showed that the PBG undergoes a slight blue shift upon an increase in the incident angle.[23] Additionally, an oblique incidence should result in an elongating optical path length in the a-Si:H layer leading to enhanced bulk absorption in the DBR or the 1D PC. The increase will thus be significant for the thinner a-Si:H layer because light absorption mainly occurs on the front surface of the first a-Si:H layer, especially for short wavelengths.

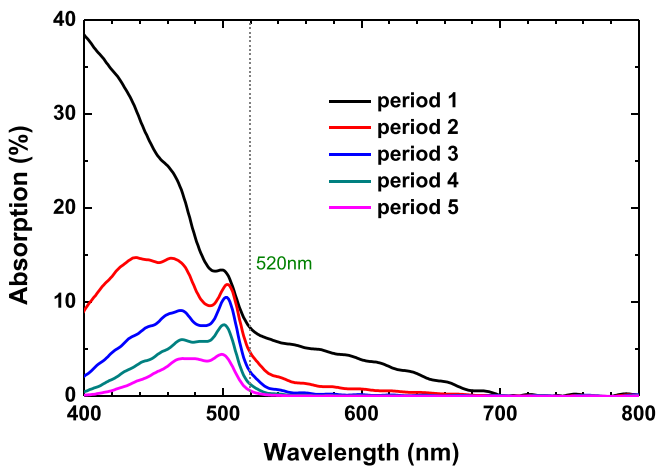

FIG. 10. Absorption spectra for individual periods in the 1D PC (from periods 1 to 5).

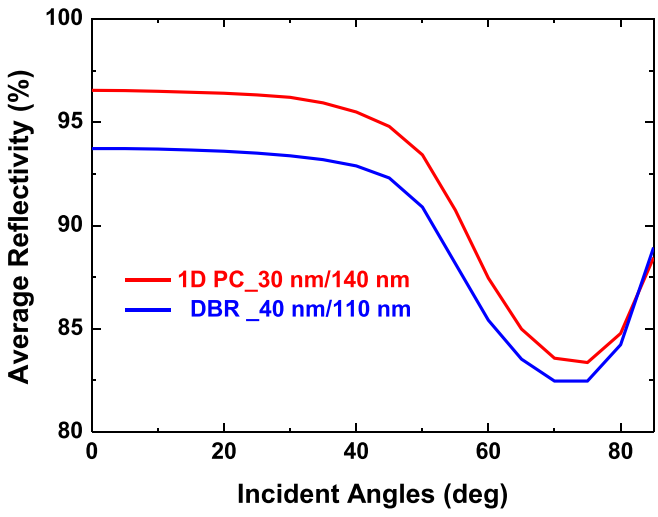

FIG. 11. Average reflectivity in the wavelength range of 520–800 nm versus the incident angle for the 1D PC with a 30 nm/140 nm and DBR structure.

The interaction of these factors results in a variation of the average reflectivity along the incident angle.

C. QE and J_{sc} increase for the 1D PC-based solar cell

As discussed before, the 1D PC structure with five periods of SiO_2 (140 nm) on top and a-Si:H (30 nm) at the bottom gives the highest reflection. Figure 12 shows a schematic structure of such a 1D PC-based *n-i-p* a-Si:H solar cell that was used in a FDTD simulation with an ITO antireflective coating as a top contact (thickness 80 nm), a *p*-μc-SiC (15 nm) as a window layer, an a-Si:H absorber layer (400 nm), a *n*-μc-SiOx (15 nm) *n*-layer followed by an aluminum-doped ZnO (AZO) back electric contact and a 1D PC back reflector. In traditional state-of-the-art TFSC, an AZO layer with a thickness of about 100 nm is inserted between the amorphous silicon and the metallic contact Ag film as part of the BR to improve its optical properties and to act as a diffusion barrier.[24,25]

To compare with the AZO/Ag BR, an AZO thickness of 100 nm was used for the 1D PC-based and the DBR-based solar cells. We placed the frequency-domain power monitor 1 at the *p*-μc-SiC/*i*-a-Si interface while monitor 2 was placed at the *i*-a-Si/*n*-μc-SiOx interface. The power absorbed by the *i*-a-Si layer (P_{abs}) was equal to the difference of the powers from monitor 1 and monitor 2. $QE(\lambda)$ was thus obtained using Eq. (2). Figure 13 shows the QE curves as a function of wavelength. Results for the solar cells based on AZO (100 nm)/Ag (100 nm) and AZO (100 nm) only were also plotted for reference. The embedded graph shows the integrated J_{sc} versus the incident angles (obliquely incident from the ITO/Air interface) for the cells based on the AZO/1D PC, the AZO/DBR and the AZO/Ag. It is clear that all the QE curves overlap each other at wavelengths less than 520 nm because of the full absorption of the intrinsic layer. With respect to the cell without a BR (AZO only), a significant increase was observed for the other three QE curves in the wavelength range of 520–800 nm. Unabsorbed sunlight penetrated the cell containing AZO (cell/AZO) only and less light was reflected back to the *i*-a-Si layer for the generation

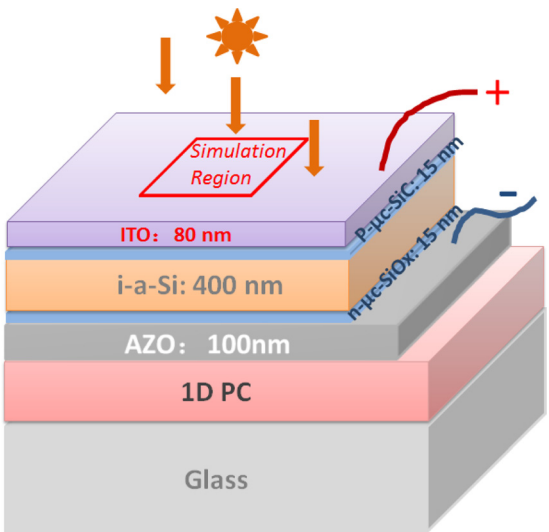

FIG. 12. Schematic of a *n-i-p* a-Si:H TFSC with a 1D PC BR structure.

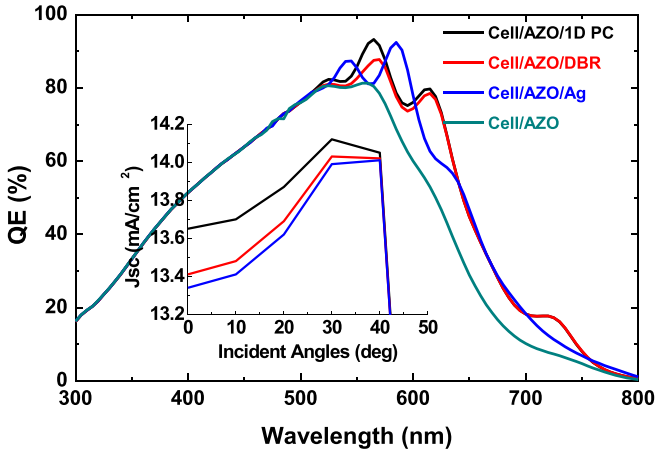

FIG. 13. QE curves for the optimized 1D PC-based TFSC, and reference cells based on DBR, AZO/Ag and AZO. The embedded graph shows the integrated J_{sc} versus incident angle for cells based on AZO/1D PC, AZO/DBR and AZO/Ag.

of interference. As a result, the QE curve for the cell/AZO was relatively smooth. When incorporating a high reflection 1D PC, a DBR or an Ag layer into the BR, the interference effect was significantly enhanced resulting in several strong oscillating peaks. The oscillating direction for the cell/AZO/Ag was different to the other three types of cells, which might come from the different phase shift of the AZO/Ag interface and the AZO/SiO_2 interface. Differences among the TFSCs of the 1D PC-based, the DBR-based and the AZO/Ag-based mainly occur in the wavelength range of 520–620 nm, which is related to their back reflection properties. Compared with the DBR-based result, the QE data improved for the optimized 1D PC-based TFSC in the wavelength range of 520–620 nm because of its higher reflection in this range, as discussed previously. Table II lists the integrated J_{sc} for the above-mentioned four configurations. The 1D PC-based TFSC offers the highest J_{sc} of 13.65 mA/cm^2, which is higher than the DBR-based cell's value of 13.41 mA/cm^2 and the AZO/Ag-based cell's value of 13.35 mA/cm^2. For the solar cell integrated with AZO only, the J_{sc} increased by a relative amount of 17.3% only upon adding the optimized 1D PC to the back.

When light is obliquely incident on an ITO/air interface, the optical path length of the intrinsic layer can be elongated leading to increased absorption. However, less light will transmit into the solar cell as the incident angle increases, which offsets the gain from an extended optical path length. Therefore, the J_{sc} values for all three types of cells shown in the embedded graph increase initially and then decrease when the angles are higher than 30° where the latter factor

TABLE II. Integrated J_{sc} of various solar cell designs based on 1D PC, DBR, AZO/Ag and AZO.

	1D PC a-Si:H/SiO_2 (30 nm/140 nm)	DBR a-Si:H/SiO_2 (40 nm/110 nm)	AZO/Ag (100 nm/100 nm)	AZO (100 nm)
J_{sc} (mA/cm^2)	13.65	13.41	13.35	11.64

becomes dominant. The back reflection effect tends to attenuate with an increase in angle because both these factors result in less light arriving at the bottom of the cell. Additionally, because of reduced index matching at the n-layer/AZO interface, a total internal reflection will occur when the incident angle of the light exceeds the critical angle of the interface. In this case, the BRs have little effect on cell performance. This helps to explain why the J_{sc} values of the three types of cells approach each other gradually with an increase in incident angle and they remain virtually the same for angles higher than 40°. In real solar cell applications, textured morphology is used for light scattering as this elongates the absorption optical path length. Additionally, cell performance is generally measured using the normal incidence. In this case, the BRs play a more important role because more light is trapped in the cell and it arrives at the interface of the cell/BR. Textured cells based on an optimal 1D PC design might improve the results more than textured cells based on the DBR structure because of their lower bulk absorption and the higher reflection of the 1D PC BR. Further investigations will be carried out into 1D PC-based textured cells. These are more complicated than flat cells and will be the topic of our next manuscript.

IV. CONCLUSION

From a PWEM simulation, three methods were found to increase the PBG: first, selecting high refractive index contrast materials; second, setting the thickness contrast to 1/2–2/3 (higher index/lower index); third, increasing the period. To enable the PBG of the 1D PC to fully cover the light trapping range needed for an a-Si:H TFSC, many groups of layer thickness contrasts (with identified materials and period thicknesses) can be used, including the DBR structure. Cross-section images of the $|E|^2$ distribution reveal that light will couple to the top three periods of the 1D PC and can be absorbed if one of the bilayers is absorptive. In this case, a good method to improve the performance of the 1D PC is to decrease the thickness contrast of the absorptive layer to the non-absorptive layer while retaining the PBG area that covers the light trapping range. An average reflectivity of 96.7% can be achieved for the 1D PC with five periods of 140 nm SiO_2 on top and a 30 nm a-Si:H layer at the bottom, which is better than the DBR structure with 93.5% and a Ag film with 93.4%. For a *n-i-p* a-Si:H TFSC with a 400 nm thick intrinsic layer, the optimal 1D PC with an AZO (100 nm) base gave the highest J_{sc} of 13.65 mA/cm^2, which is superior to the AZO/DBR-based cell with 13.41 mA/cm^2 and the AZO/Ag-based cell with 13.35 mA/cm^2.

ACKNOWLEDGMENTS

This research is supported by the National Natural Science Foundation of China (Nos. 61176060 and 61377031), the Key Project of Natural Science Foundation of Tianjin (No. 12JCZDJC28300), the National High-tech R&D Program of China (No. 2011AA050503), the National Basic Research Program of China (Nos. 2011CBA00705, 2011CBA00706, and 2011CBA00707) and the Major Science and Technology Support Project of Tianjin (No. 11TXSYGX22100).

[1]C. M. Hsu, C. Battaglia, C. Pahud, Z. C. Ruan, F. J. Haug, S. H. Fan, C. Ballif, and Y. Cui, Adv. Energy Mater. **2**, 628 (2012).
[2]A. Shah, P. Torres, R. Tscharner, N. Wyrsch, and H. Keppner, Science **285**, 692 (1999).
[3]J. Muller, B. Rech, J. Springer, and M. Vanecek, Solar Energy **77**, 917 (2004).
[4]Z. F. Yu, A. Raman, and S. H. Fan, Opt. Express **18**, A366 (2010).
[5]G. Yue, L. Sivec, J. M. Owens, B. Yan, J. Yang, and S. Guha, Appl. Phys. Lett. **95**, 263501 (2009).
[6]T. Soderstrom, F. J. Haug, X. Niquille, and C. Ballif, Prog. Photovolt. **17**, 165 (2009).
[7]V. E. Ferry, M. A. Verschuuren, M. C. van Lare, R. E. I. Schropp, H. A. Atwater, and A. Polman, Nano Lett. **11**, 4239 (2011).
[8]A. Micco, A. Ricciardi, M. Pisco, V. La Ferrara, L. V. Mercaldo, P. D. Veneri, A. Cutolo, and A. Cusano, J. Appl. Phys. **114**, 063103 (2013).
[9]B. Curtin, R. Biswas, and V. Dalal, Appl. Phys. Lett. **95**, 231102 (2009).
[10]R. Biswas, J. Bhattacharya, B. Lewis, N. Chakravarty, and V. Dalal, Solar Energy Mater. Solar Cells **94**, 2337 (2010).
[11]O. Isabella, S. Dobrovolskiy, G. Kroon, and M. Zeman, J. Non-Crystall. Solids **358**, 2295 (2012).
[12]L. Zeng, P. Bermel, Y. Yi, B. A. Alamariu, K. A. Broderick, J. Liu, C. Hong, X. Duan, J. Joannopoulos, and L. C. Kimerling, Appl. Phys. Lett. **93**, 221105 (2008).
[13]P. G. O'Brien, N. P. Kherani, A. Chutinan, G. A. Ozin, S. John, and S. Zukotynski, Adv. Mater. **20**, 1577 (2008).
[14]C. Lopez, Adv. Mater. **15**, 1679 (2003).
[15]D. Y. Zhou and R. Biswas, J. Appl. Phys. **103**, 093102 (2008).
[16]L. Zeng, Y. Yi, C. Hong, J. Liu, N. Feng, X. Duan, L. C. Kimerling, and B. A. Alamariu, Appl. Phys. Lett. **89**, 111111 (2006).
[17]P. Bermel, C. Luo, L. Zeng, L. C. Kimerling, and J. D. Joannopoulos, Opt. Express **15**, 16986 (2007).
[18]S. Y. Shi, C. H. Chen, and D. W. Prather, J. Opt. Soc. Am. A **21**, 1769 (2004).
[19]M. Loncar, T. Doll, J. Vuckovic, and A. Scherer, J. Lightwave Technol. **18**, 1402 (2000).
[20]See http://rredc.nrel.gov/solar/spectra/am1.5/ASTMG173/ASTMG173.html for ASTMG173-03, Standard Tables for Reference Solar Spectral Irradiances: Direct Normal and Hemispherical on 37 degree Tilted Surface (ASTM International, West Conshohocken, Pennsylvalia, 2005).
[21]C. Rockstuhl, S. Fahr, and F. Lederer, J. Appl. Phys. **104**, 123102 (2008).
[22]X. Wang, X. H. Hu, Y. Z. Li, W. L. Jia, C. Xu, X. H. Liu, and J. Zi, Appl. Phys. Lett. **80**, 4291 (2002).
[23]P. Z. Chen, G. F. Hou, S. Suo, J. Ni, J. J. Zhang, X. X. Zhang, and Y. Zhao, Acta Phys. Sin. **63**, 128801 (2014).
[24]B. Yan, G. Yue, L. Sivec, J. Owens-Mawson, J. Yang, and S. Guha, Solar Energy Mater. Solar Cells **104**, 13 (2012).
[25]F. J. Haug, T. Soederstroem, O. Cubero, V. Terrazzoni-Daudrix, and C. Ballif, J. Appl. Phys. **104**, 064509 (2008).